AGU PUBLICATIONS

Geophysical Research Letters

RESEARCH LETTER
10.1002/2017GL073939

Key Points:
- Algorithm to retrieve dust optical depth and centroid height using the O_2 A and B bands is developed
- First retrieval results of dust optical depth and altitude from EPIC/DSCOVR are shown in good agreement with the counterparts from MODIS and CALIPSO
- Passive remote sensing of aerosol height multiple times within a day is demonstrated with EPIC and discussed for future studies

Supporting Information:
- Supporting Information S1

Correspondence to:
J. Wang and X. Xu,
jun-wang-1@uiowa.edu;
xiaoguang-xu@uiowa.edu

Citation:
Xu, X., J. Wang, Y. Wang, J. Zeng, O. Torres, Y. Yang, A. Marshak, J. Reid, and S. Miller (2017), Passive remote sensing of altitude and optical depth of dust plumes using the oxygen A and B bands: First results from EPIC/DSCOVR at Lagrange-1 point, *Geophys. Res. Lett.*, *44*, 7544–7554, doi:10.1002/2017GL073939.

Received 28 APR 2017
Accepted 5 JUL 2017
Accepted article online 10 JUL 2017
Published online 30 JUL 2017
Corrected 6 SEP 2017

This article was corrected on 6 SEP 2017. See the end of the full text for details.

Passive remote sensing of altitude and optical depth of dust plumes using the oxygen A and B bands: First results from EPIC/DSCOVR at Lagrange-1 point

Xiaoguang Xu[1], Jun Wang[1], Yi Wang[1], Jing Zeng[1], Omar Torres[2], Yuekui Yang[3], Alexander Marshak[3], Jeffrey Reid[4], and Steve Miller[5]

[1]Department of Chemical and Biochemical Engineering, Center for Global and Regional Environmental Studies, and Informatics Initiative, University of Iowa, Iowa City, Iowa, USA, [2]Atmospheric Chemistry and Dynamics Laboratory, NASA Goddard Space Flight Center, Greenbelt, Maryland, USA, [3]Climate and Radiation Laboratory, NASA Goddard Space Flight Center, Greenbelt, Maryland, USA, [4]Marine Meteorology Division, Naval Research Laboratory, Monterey, California, USA, [5]Cooperative Institute for Research in the Atmosphere, Colorado State University, Fort Collins, Colorado, USA

Abstract We presented an algorithm for inferring aerosol layer height (ALH) and optical depth (AOD) over ocean surface from radiances in oxygen A and B bands measured by the Earth Polychromatic Imaging Camera (EPIC) on the Deep Space Climate Observatory (DSCOVR) orbiting at Lagrangian-1 point. The algorithm was applied to EPIC imagery of a 2 day dust outbreak over the North Atlantic Ocean. Retrieved ALHs and AODs were evaluated against counterparts observed by Cloud-Aerosol Lidar with Orthogonal Polarization (CALIOP), Moderate Resolution Imaging Spectroradiometer, and Aerosol Robotic Network. The comparisons showed 71.5% of EPIC-retrieved ALHs were within ±0.5 km of those determined from CALIOP and 74.4% of EPIC AOD retrievals fell within a ± (0.1 + 10%) envelope of MODIS retrievals. This study demonstrates the potential of EPIC measurements for retrieving global aerosol height multiple times daily, which are essential for evaluating aerosol profile simulated in climate models and for better estimating aerosol radiative effects.

Plain Language Summary DSCOVR is a satellite parked at Lagrange-1 point, ~1.5 million kilometers from Earth. It was launched in February 2015 and started the data collection in June 2015. It carries a sensor called EPIC that looks at the sunlit surface every 1 to 2 h. This paper presents a new technique to retrieve dust optical depth and dust altitude from EPIC's measurements within and outside of oxygen A and B absorption bands. The results are validated with MODIS and CALIOP data. The technique represents, for the first time, that we can reliably retrieve dust plume height from passive remote sensing multiple times a day.

1. Introduction

Vertical distribution of atmospheric aerosols influences the Earth's climate and environment in many ways. First, absorption of solar and terrestrial radiation by smoke and dust particles modifies the air thermal state and stability, and the resulting effect on the atmospheric stability depends on the altitude of aerosol layers [*Babu et al.*, 2011; *Wendisch et al.*, 2008; *Zhu et al.*, 2007]. Second, the altitude of absorbing particles relative to clouds can influence cloud cover and lifetime [*Koch and Del Genio*, 2010; *Satheesh et al.*, 2008; *Ge et al.*, 2014]. Thus, aerosol vertical distribution can affect the magnitude and even the sign of aerosol direct and indirect radiative effects [*Choi and Chung*, 2014; *Samset et al.*, 2013]. However, centroid altitude of aerosol layers simulated by current climate models can differ by up to an order of magnitude in the range of 1.5 km to 3 km [*Koffi et al.*, 2012; *Kipling et al.*, 2016], leading to considerable uncertainty in the estimated aerosol radiative forcing. Furthermore, elevated dense aerosol plumes such as lofted mineral dust and volcanic ash, which are invisible to the aircraft radar, can pose significant hazards on aviation safety [*Sears et al.*, 2013]. Therefore, it is critically important to observe the vertical distribution of aerosols on a global scale.

Detailed profile of attenuated backscatter can be probed by active remote sensing techniques using lidar, such as the Cloud-Aerosol Lidar with Orthogonal Polarization (CALIOP) [*Winker et al.*, 2009]. However, the spatial coverage of CALIOP measurements suffers from its narrow swath. The gap between its adjacent suborbital "curtains" is as wide as 2200 km, especially in the tropics and subtropics. By contrast, passive remote sensing techniques provide adequate spatial coverage but poor vertical resolution and have been mainly used to retrieve columnar aerosol quantities in cloud-free scenes. Nevertheless, various passive techniques

have been developed to retrieve limited but useful information of aerosol altitude [*Xu et al.*, 2017]. While not achieving the same level of accuracy as a lidar, passive techniques can add an important augmentation due to the better spatial coverage.

One passive technique utilizes absorption spectroscopy of molecular oxygen (O_2) [e.g., *Zeng et al.*, 2008; *Dubuisson et al.*, 2009; *Kokhanovsky and Rozanov*, 2010; *Sanders et al.*, 2015; *Ding et al.*, 2016]. Its physical principle relies on that the aerosol layer can scatter photons back to space and reduce the chance of a photon being absorbed by the underlying O_2 molecules. A risen scattering layer increases the chance for photons to be scattered, enhancing the reflectivity in the O_2 absorption bands as detected by a satellite [*Dubuisson et al.*, 2009; *Wang et al.*, 2014]. Therefore, spectral characteristics of reflectance in O_2 bands can manifest how aerosol particles interact with O_2 absorption through multiple scattering at different altitudes. With this principle, attempts have been made to retrieve aerosol height using observations in the O_2 A band from low-Earth-orbiting (LEO) instruments including POLDER (Polarization and Directionality of the Earth's Reflectances) and MERIS (Medium Resolution Imaging Spectrometer) [*Dubuisson et al.*, 2009], SCIAMACHY (SCanning Imaging Absorption spectroMeter for Atmospheric CHartographY) [*Kokhanovsky and Rozanov*, 2010; *Sanghavi et al.*, 2012], and GOME/GOME-2 (Global Ozone Monitoring Experiment) [*Koppers and Murtagh*, 1997; *Sanders et al.*, 2015]. Overall, these studies showed that the height of aerosol layers over ocean can be properly retrieved when aerosol layers are in the free troposphere. The height information for aerosols within boundary layers is limited but can be enhanced by combining O_2 A and B bands in which O_2 absorption strengths are different [*Pflug and Ruppert*, 1993; *Ding et al.*, 2016]; such enhancement was shown primarily through theoretical studies but with limited analysis of real data and validation [*Sanghavi et al.*, 2012].

On 11 February 2015, NASA launched the Deep Space Climate Observatory (DSCOVR), which carries the Earth Polychromatic Imaging Camera (EPIC) to observe Earth-reflected solar radiation in 10 narrow channels covering both the O_2 A and B bands [*Marshak and Knyazikhin*, 2017]. DSCOVR flies on the Lissajous orbit about 1.5×10^6 km away at the Lagrange-1 point, giving EPIC a unique angular perspective at an almost constant scattering angle between 165° and 178°. EPIC scans the entire sunlit face of the Earth at a 2048×2048 pixel resolution, rendering the pixel size of 12×12 km^2 at the image center. In contrast to LEO sensors that observe a location once a day, EPIC can track the change of aerosol layer height multiple times a day. Also, EPIC provides a finer spatial resolution and wider coverage than LEO sensors that include both O_2 A and B bands, i.e., 80×40 km^2 for GOME-2 and 30×60 km^2 for SCIAMACHY.

This paper describes an algorithm that, for the first time, uses real measurements in O_2 A and B bands from EPIC to estimate the centroid altitude and optical depth of aerosols residing over a water background. We demonstrated the algorithm through applying it to dust plumes over the North Atlantic Ocean for two adjacent days and evaluated the retrievals with a comprehensive use of MODIS (Moderate Resolution Imaging Spectroradiometer), AERONET (Aerosol Robotic Network), and CALIOP data. This paper is outlined as follows. The specifics of the EPIC sensor are introduced in section 2, the retrieval method is described in section 3, and the case study and validation are presented in section 4. Finally, we summarize the findings and consider future research in section 5.

2. EPIC Measurements

EPIC measures Earth-reflected solar radiance in 10 narrow bands spanning from UV to near-infrared spectrum, which include four channels around the O_2 A and B. As shown in Figure S1, two absorption channels are centered at 688 nm and 764 nm with bandwidth of 0.8 nm and 1.0 nm, respectively. Two continuum bands are placed at 680 nm and 780 nm. These bands were designed for monitoring vegetation condition [*Marshak and Knyazikhin*, 2017] and cloud height [*Yang et al.*, 2013].

We used EPIC Level 1b (L1B) version-1 radiance made available from https://eosweb.larc.nasa.gov. Various prelaunch and postlaunch calibrations were applied to the L1B EPIC data [*Cede and Kowalewski*, 2016]. EPIC visible channels were cross calibrated with LEO instruments like MODIS and VIIRS (Visible Infrared Imaging Radiometer Suite) [*Haney et al.*, 2016]. The two O_2 absorption channels were calibrated by lunar surface reflectivity [*Herman et al.*, 2016]. The top-of-the-atmosphere (TOA) reflectance is calculated by

$$\rho_\lambda = \pi \frac{I(\lambda)}{\mu_0 E_0(\lambda)}, \tag{1}$$

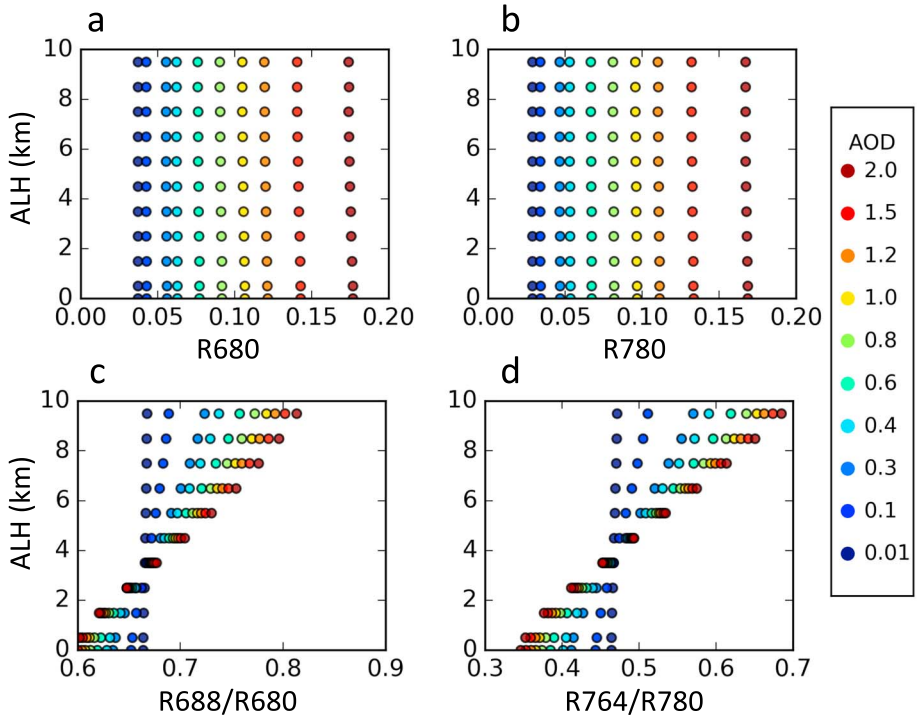

Figure 1. Relationship between ALH and TOA reflectance in two EPIC continuum bands at (a) 680 nm and (b) 780 nm for various AOD values. (c and d) Relationship between ALH and reflectance ratio in the EPIC O_2 A and B bands for various AOD values. Simulations are performed for dust aerosol optical property (Figure S3) under the following conditions: a solar zenith angle of 42°, a view zenith angle of 31°, a relative azimuth angle of 0° (backscatter), and a surface reflectance of 0.015. Note the colors of dots indicate different AOD values.

where $I(\lambda)$ and $E_0(\lambda)$ are, respectively, EPIC-measured radiance and solar irradiance at wavelength of λ, and μ_0 is the cosine of solar zenith angle.

3. Methodology

3.1. Radiative Transfer Modeling and Retrieval Principle

To construct the relationship between EPIC measurements and aerosol vertical profile, TOA reflectance was simulated using the Unified Linearized Vector Radiative Transfer Model (UNL-VRTM) [*Wang et al.*, 2014]. UNL-VRTM couples the VLIDORT [*Spurr*, 2006] radiative transfer code to the HITRAN molecular spectroscopic database [*Rothman et al.*, 2009] and aerosol scattering codes. The solar irradiance reference spectrum from *Chance and Kurucz* [2010] was applied. Radiance was then obtained by convolving simulated hyperspectral monochromatic radiances with EPIC instrument filter functions for 680, 688, 764, and 780 nm bands.

We assumed a Gaussian-like aerosol profile characterized by a columnar aerosol optical depth (AOD), centroid altitude, and a half-width parameter (Equation (S1) and Figure S2 in the supporting information) [*Spurr and Christi*, 2014]. The centroid altitude was used to represent aerosol layer height (ALH). Aerosol single scattering properties at EPIC bands were determined from the AERONET inversion products that treat dust particles as spheroids [*Holben et al.*, 1998; *Dubovik et al.*, 2006]. Following *Xu et al.* [2015], we compiled AERONET version-2 inversion data over Capo_Verde site retrieved for 2015 and determined the climatological single-scattering albedo (SSA) and phase function (Figure S3), as well as Ångstrom exponent (AE) between 675 and 870 nm, in the dusty conditions when coarse-mode volume fraction is larger than 0.6 and 440 nm AOD above 0.4.

Figure 1 shows the relationship between dust ALH and reflectance (and ratio) in EPIC O_2 bands for various AOD values. Those simulations were performed for an ocean surface with reflectance of 0.015 at an EPIC geometry of $[\theta_0, \theta, \phi] = [42°, 31°, 0°]$, where θ_0 and θ are solar and view zenith angles, and ϕ the relative

azimuth angle. As seen from the figure, while reflectance in the continuum bands is sensitive to AOD but not to ALH (Figures 1a and 1b), ratios of reflectance of the absorption-to-continuum bands are sensitive to both AOD and ALH (Figures 1c and 1d). The higher the aerosol layer, the larger the reflectance ratio; this can be explained that a higher scattering layer gives more chance for photons being scattered and increases reflectance in the absorption band. Meanwhile, sensitivity of the reflectance ratio to ALH decreases as AOD decreases and diminishes as AOD approaches zero. Additional simulations with different surface reflectance and viewing geometry were also performed (not shown), which were found to be consistent with previous studies in that the sensitivity of reflectance ratio to ALH decreased with an increase of surface reflectance and varied with geometry [*Boesche et al*., 2009; *Dubuisson et al*., 2009; *Wang et al*., 2014; *Ding et al*., 2016].

Our algorithm retrieves ALH and AOD from EPIC measurements in the context of lookup tables (LUTs) that contain TOA reflectance at EPIC bands simulated for a set of predefined ALH and AOD values and for various surface reflectance and satellite geometries: (1) 680 nm AOD values of 0.01, 0.1, 0.3, 0.4, 0.6, 0.8, 1.0, 1.2, 1.5, 2.0, and 3.0; (2) ALH from 0 to 15 km with 1 km intervals and half width of 1 km; (3) surface reflectance values of 0, 0.015, 0.03, 0.05, and 0.1; and (4) θ_0 and θ from 0° to 78° with 6° intervals and $|\theta_0 - \theta| < 15°$ (EPIC backscatter), and ϕ from 0° to 180° with 12° intervals.

The assumed half width of 1 km is representative of an average profile observed by Lidar for dust and smoke aerosols [*Reid et al*., 2003]. This value was also used to derive AOD from UV observations by TOMS (Total Ozone Mapping Spectrometer) and OMI (Ozone Monitoring Instrument) [*Torres et al*., 1998].

3.2. Retrieval Procedures

Our retrieval algorithm performs a simultaneous inversion of four EPIC channels (680, 688, 764, and 780 nm) to solve AOD and ALH. In brief, it entails three steps. First, we aggregated EPIC imagery into $0.1° \times 0.1°$ grids using nearest-neighbor interpolation for the entire 10 channels. Georegistration of EPIC radiance is different from one band to another because monochromatic imagery is taken sequentially while the Earth is rotating. This step ensures a consistent geographical coordinate across EPIC bands. The retrieval results are also delivered at the aggregated grids.

The second step involves screening of cloud and sunglint to identify pixels that are suitable for aerosol retrieval. The sunglinted area over ocean with a glint angle smaller than 30° was removed [*Levy et al*., 2013]. Cloud pixels were screened out through brightness and homogeneity tests [*Martins et al*., 2002], which is illustrated in Figure S4. However, thin and small subpixel clouds can be easily overlooked from 12 km EPIC pixels, leading to an overestimated AOD and underestimated ALH (Figures 1c and 1d). Therefore, cloud screening is a potential issue to the retrieval quality, and one that may benefit from enlisting higher-resolution geostationary sensors' cloud mask information for future efforts.

Finally, ALH and AOD were determined from EPIC observations in the context of LUTs. We first interpolated LUTs over EPIC observation geometry and surface reflectance determined by GOME-2 surface Lambert-equivalent reflectivity database [*Koelemeijer et al*., 2003]. Based on the interpolated LUT, we refined the AOD grid with 0.01 intervals and the ALH grid with 0.1 km intervals and interpolated reflectance for the refined AOD and ALH values. The inverse problem was then formulated in a way that the optimal values of AOD and ALH corresponded to the minimization of a scalar cost function

$$\epsilon = \sqrt{\frac{1}{4}\sum_{i=1}^{4}[y_i - F_i(\mathbf{x})]^2}, \tag{2}$$

where y_i is the EPIC reflectance in band i, $\mathbf{x}$ is a state vector comprising ALH and AOD, and $F_i(\mathbf{x})$ is the LUT reflectance in band i for any given $\mathbf{x}$. The ϵ parameter was reported along with the retrieved ALH and AOD and can be an indicator of retrieval quality (Figure S5).

4. Application to EPIC Imagery Over Marine Surfaces

4.1. Retrieval Results

Our case study focused on dust plumes over subtropical North Atlantic Ocean. Saharan dust is often transported across this region before reaching the Caribbean Sea [*Prospero et al*., 2002; *Yu et al*., 2010, 2015]. The vertical structure and dynamics of the dust layer over this region are controlled by large-scale

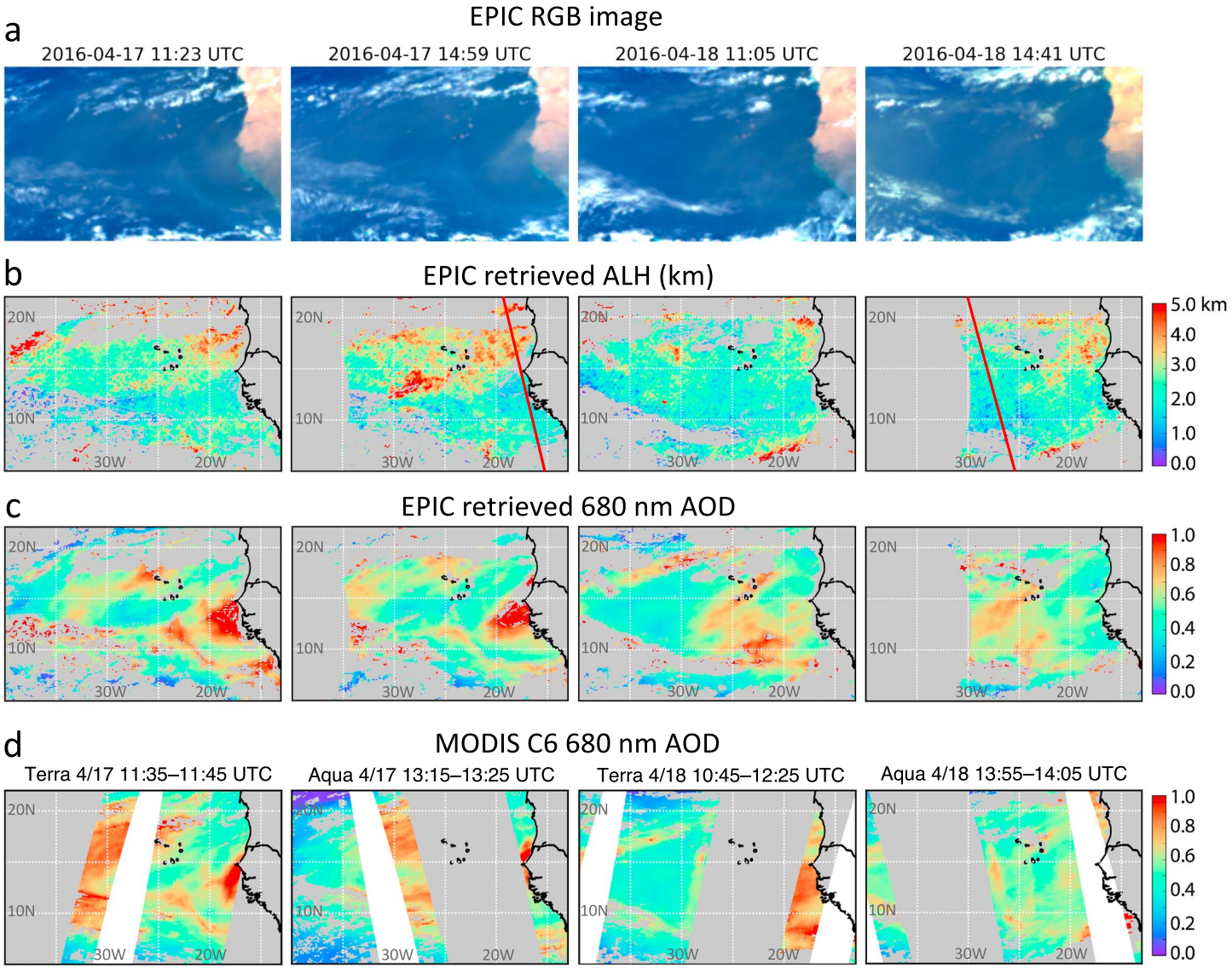

Figure 2. Retrieval results for dust plumes from four EPIC images during 17–18 April 2016. (a) Enhanced RGB images created using EPIC measurements at 680 nm, 551 nm, and 440 nm. (b) Aerosol layer height (ALH) retrieved from EPIC measurements when AOD is over 0.3. Red lines indicate CALIPSO suborbital track for the same day overpass. (c) EPIC retrieved aerosol optical depth (AOD) at 680 nm. (d) MODIS level 2 AOD (collection 6) from both Terra and Aqua satellites, which were spectrally interpolated from 0.66 μm and 0.87 μm to 680 nm using Ångstrom exponent (AE).

atmospheric circulation and regional-scale convection [*Karyampudi et al.*, 1999; *Reid et al.*, 2002, 2003; *Huang et al.*, 2010; *Yu et al.*, 2010, 2015]. In late spring and summer, dust aerosols are lofted from the Sahara deserts by strong sensible heating and low-level convergence and travel along with trade winds in a warm and dry air mass known as the Saharan Air Layer (SAL) [*Prospero and Carlson*, 1972]. Typically, the SAL extends from 1 km to 6 km with dust concentration peaked between 1.5 and 3.7 km. The top altitude of the SAL descends as air travels away from the African coast [*Carlson and Prospero*, 1972; *Karyampudi et al.*, 1999; *Maring et al.*, 2003; *Colarco et al.*, 2003], a characteristic that is likely related to the subtropical subsidence [*Huang et al.*, 2010]. Regional subsidence can also bring elevated dust aerosols into marine boundary layer [*Colarco et al.*, 2003]. As a result, dust altitude in North Atlantic Ocean is subject to large seasonal and spatial variability [*Huang et al.*, 2010; *Yu et al.*, 2010, 2015].

We applied our algorithm to four EPIC scenes acquired on 17–18 April 2016, which provided optimal comparison with MODIS and CALIOP observations (section 4.2). In the EPIC RGB images (Figure 2a), dust outflows appeared as light brown plumes over the dark marine surface. The retrievals of ALH, shown in Figure 2b,

manifested strong spatial variability. In the northwest African coast, ALH ranged from 3 km to 5 km in the area north of 15°N but decreased to about 2 km toward south. This variation was likely controlled by large-scale circulation. As shown in Figure S6, strong upward air motions coincided with high ALH in the area north of 15°N, and low ALH at lower latitudes was associated with subtropical subsidence of Intertropical Convergence Zone's northern branch. This is consistent with the study by *Karyampudi et al*. [1999], who showed that intense sensible heating in the Sahara could produce strong dry convection uplifting dust from the surface to SAL [*Carlson and Prospero*, 1972]. As dust aerosols transported off the coast, SAL altitude gradually descended. On diurnal basis, higher ALH were found in the afternoon, which might be related to diurnal evolution of tropospheric convection.

Figure 2c shows retrieved 680 nm AOD, which clearly illustrate the transport of dust. On 17 April, dust plumes with large AOD values moved off the Saharan coast toward southeast. On the second day, dispersed dust plumes were found over Cape Verde and extended to 30°W. In addition, scattered retrievals with AOD larger than 1 were found around 12°N between 40°W and 30°W, which were possibly contaminated by subpixel clouds.

4.2. Comparison of AOD Retrievals With MODIS and AERONET

We first compared EPIC retrieved AOD with MODIS Collection 6 level-2 10 km AOD products [*Remer et al*., 2005; *Levy et al*., 2013]. Products from both Terra and Aqua satellites were used to evaluate EPIC retrievals in local morning and afternoon, respectively. The expected uncertainty of MODIS AOD was claimed to be (+(0.04 + 10%), −(0.02 + 10%)) over ocean [*Levy et al*., 2013]. However, MODIS ocean AOD retrieval assumes spherical aerosols which, in the case of dust, can cause larger and angular-dependent biases [*Levy et al*., 2003]. A recent evaluation by *Banks et al*. [2017] indicated such retrieval bias can be as large as +0.13. Therefore, it should be emphasized that MODIS AODs did not serve as ground truth for validating EPIC retrievals. Rather, they were used for an intercomparison.

Figure 2d shows MODIS AOD at 680 nm, which were spectrally interpolated from 0.66 to 0.87 μm. In comparison, EPIC retrievals (Figure 2c) exhibited wider spatial coverage and captured the overall pattern of dust plumes as identified by MODIS. Meanwhile, regional disparities were present between EPIC and MODIS AODs, which could be caused by differences in the effectiveness of cloud masking, used aerosol models, and observation time. EPIC, with pixel size over 10 times larger, was more likely to be contaminated by thin- and small-scale clouds. Also, our EPIC algorithm used a nonspherical dust aerosol model, whereas MODIS aerosol algorithm combined a fine and a coarse spherical aerosol mode. In addition, there were up to 1 h time differences between MODIS and EPIC observations. Rapidly evolving dust plumes could result in substantial diurnal variations of AOD [*Wang et al*., 2003].

Figure 3a shows a scatterplot of EPIC AOD versus MODIS AOD, both aggregated into a 0.5° × 0.5° grid. In total, 74.7% of the EPIC retrievals fell within a ± (0.1 + 10%) envelope of MODIS AOD. EPIC AOD captured 36% variance of the MODIS AOD with a root-mean-square error (RMSE) of 0.15. The metric of ±(0.1 + 10%) was selected to indicate an expected uncertainty level of EPIC AOD. This uncertainty is larger than that claimed for MODIS over ocean AOD [*Levy et al*., 2013] to account for a more acute cloud contamination.

AERONET version-2 AOD observations [*Holben et al*., 1998] were used to validate EPIC retrievals over Calhau, Capo_Verde, and Dakar sites. Site location and time series of AERONET AOD and collocated EPIC retrievals are illustrated in Figure S7. Observed AE at these AERONET sites was below 0.2 throughout the study period, indicating the overwhelming of dust aerosols. Figure 3b presents a scatterplot of collocated EPIC and MODIS retrievals versus AERONET AODs. The collocation method follows *Ichoku et al*. [2002] but was updated to associate a subset of satellite retrievals within a 0.5° × 0.5° grid centered at each site to a subset of 1 h AERONET observations around satellite overpass time. The collocated EPIC retrievals, though with limited data samplings, all fell within the ±(0.1 + 10%) envelope of AERONET AOD with a RMSE of 0.07 and a coefficient of determination (R^2) of 0.81. This represents a better performance than MODIS retrievals (with RMSE of 0.09 and R^2 of 0.68). The positive bias in EPIC AOD was 0.02. This bias was dominated for two subsets of EPIC AODs with large spatial variation (Figures 3b and S7), which was likely caused by cloud contamination.

4.3. Validation of ALH Retrievals With CALIOP Observations

To validate EPIC retrieved ALH, we used CALIOP level-2 aerosol extinction profiles at a spatial resolution of 60 m vertically and 5 km horizontally, which were retrieved from CALIOP attenuated backscatter at

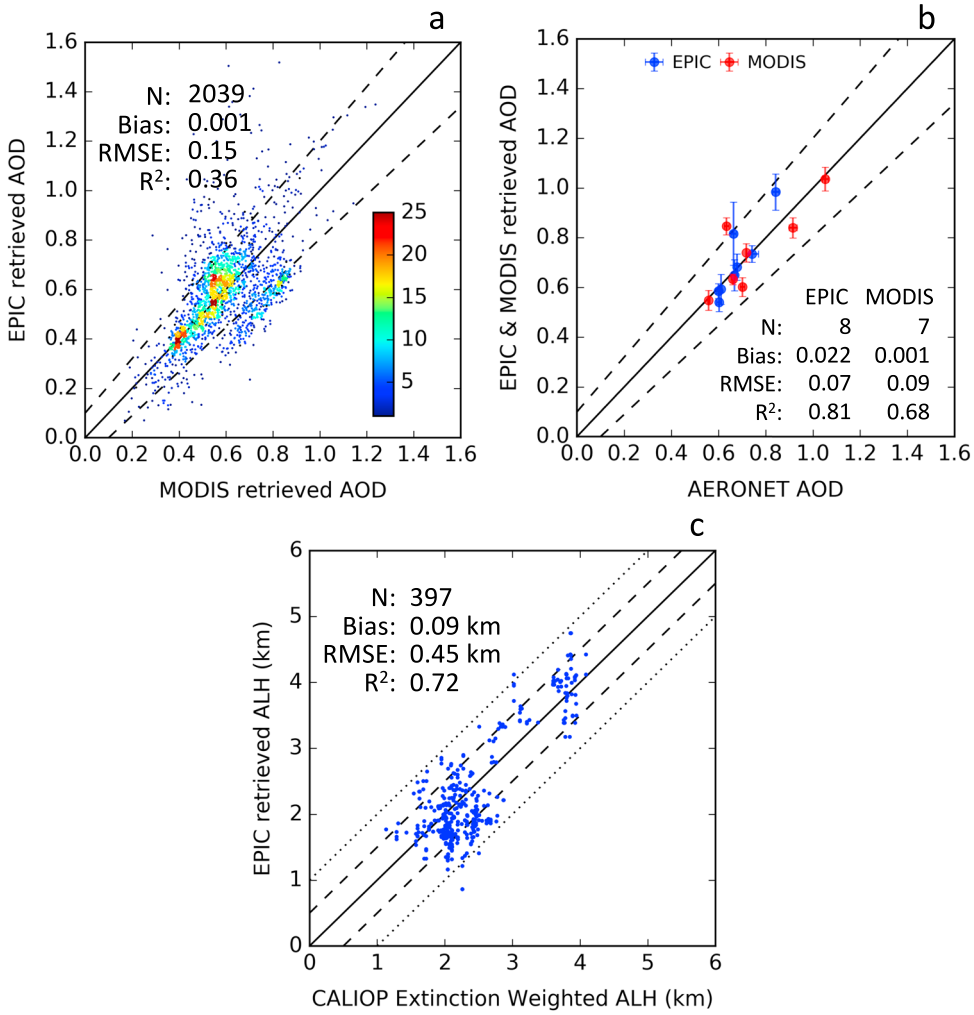

Figure 3. Comparison of EPIC retrieved AOD and ALH with the counterparts from MODIS, AERONET, and CALIOP measurements. (a) Scatterplot of EPIC retrieved 680 nm AOD versus MODIS C6 680 nm AOD, both aggregated into a 0.5° spatial resolution. Each scatter indicates an AOD pair over a 0.5° × 0.5° grid. Color of scatter indicates the frequency of scatters falling within 0.025 AOD intervals. Also shown are one-by-one line (solid) and ±(0.1 + 10%) (dashed) envelop. (b) Scatterplot of EPIC 680 nm AOD (blue) and MODIS 680 nm AOD (red) versus AERONET 675 nm AOD. Error bars indicate standard deviation of sampled subsets. One-by-one line and ±(0.1 + 10%) envelope are indicated by solid and dashed lines, respectively. (c) Scatterplot of EPIC retrieved ALH versus CALIOP extinction-weighted ALH sampled for cloud-free conditions. Also plotted are one-by-one line (solid), ±0.5 km (dashed) and ±1.0 km (dotted) envelops. Annotated in each panel are number of samples (N), bias, root-mean-square error (RMSE), and coefficient of determination (R^2).

532 nm [*Young and Vaughan*, 2009]. To facilitate quantitative comparison, a mean ALH was calculated from the CALIOP extinction profile following *Koffi et al.* [2012]

$$\mathrm{ALH_{CALIOP}} = \frac{\sum_{i=1}^{n} \beta_{\mathrm{ext},i} Z_i}{\sum_{i=1}^{n} \beta_{\mathrm{ext},i}}. \tag{3}$$

Here $\beta_{\mathrm{ext},i}$ is aerosol extinction coefficient (km^{-1}) at level i with an altitude of Z_i (km). n is 166 for the considered top level at 10 km. Thus, $\mathrm{ALH_{CALIOP}}$ represents an effective ALH weighted by aerosol extinction signal at each level and is directly comparable with ALH defined in our retrieval algorithm.

Figure 4 compares EPIC-retrieved ALH (black) and CALIOP extinction profiles. The Cloud-Aerosol Lidar and Infrared Pathfinder Satellite Observation (CALIPSO) suborbital track was along the coastal marine surface on 17 April and moved toward west on the next day (Figure 2b). As evident in CALIOP profiles, the spatial

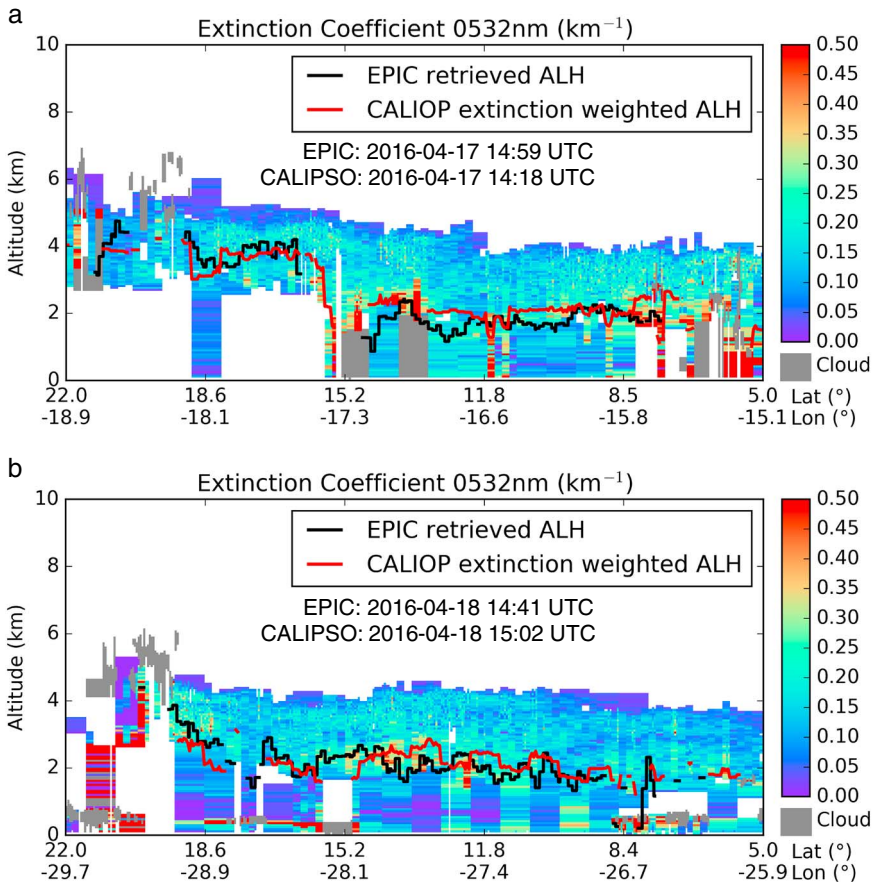

Figure 4. Validation of EPIC ALH (black curve) with CALIOP profile of 532 nm extinction coefficient acquired on (a) 17 and (b) 18 April. The corresponding suborbital tracks are indicated in Figure 2b. Cloud layers are indicated by gray color. The red curve depicts CALIOP extinction-weighted ALH calculated by equation (3).

variability of EPIC-retrieved ALH generally agreed with that observed by CALIOP. On 17 April, elevated dust layers appeared between 3 km and 6 km in the area north to 15°N. At lower latitudes, aerosol layers extended from the surface to about 4 km. Correspondingly, the ALH_{CALIOP} was about 4 km in the north and 2 km at lower latitudes. On 18 April, ALH_{CALIOP} gradually decreased from about 3 km in the north to 2 km at lower latitudes. A scatterplot of EPIC ALH versus ALH_{CALIOP} in cloud-free scenes is shown in Figure 3c. We found 71.5% and 98.7% of EPIC ALH retrievals were located within ±0.5 km and ±1.0 km envelops of ALH_{CALIOP}, respectively. The variability of EPIC ALH explained 72% variance of ALH_{CALIOP} with a RMSE of 0.45 km. Therefore, we expect that the accuracy of EPIC-retrieved ALH is better than 0.5 km.

5. Discussion and Conclusion

In this paper, we presented a new retrieval algorithm that infers aerosol layer height (ALH) and optical depth (AOD) from backscattered radiation in O_2 A and B bands observed by the EPIC/DSCOVR orbiting around the Lagrange-1 point. The algorithm was applied to EPIC imagery for dust plumes acquired over North Atlantic Ocean during 17–18 April 2016. We found that EPIC-retrieved ALHs were in good agreement with CALIOP-probed aerosol extinction profile, with 71.5% of EPIC retrievals falling within ±0.5 km of CALIOP extinction-weighted altitude and a RMSE of 0.45 km. Thus, retrieval accuracy of EPIC ALH is expected to be better than 0.5 km. EPIC AOD retrievals were well validated by AERONET AOD. The AOD retrievals agreed with MODIS AOD in that 74.7% of EPIC AOD retrievals are in a ± (0.1 + 10%) envelope of MODIS AOD.

The implication of this study is twofold. First, EPIC observations can provide global aerosol height information multiple times a day, which will allow further study of diurnal variation of aerosol vertical structure. Such

information is valuable for evaluating the vertical distribution of aerosols estimated by climate models [*Koffi et al*., 2012] and for better estimating aerosol radiative effects [*Zhang et al*., 2013]. Second, the retrieved ALH can provide complementary height information for determining absorbing aerosol properties from UV bands. EPIC also measures backscattered UV radiances at 340 nm and 388 nm, which was designed to detect UV-absorbing aerosols like mineral dust and smoke [*Torres et al*., 2016]. However, inferring aerosol properties from those UV bands requires the characterization of aerosol height, because UV radiance is sensitive to aerosol vertical distribution [*Torres et al*., 1998]. For example, *Jeong and Hsu* [2008] retrieved SSA from OMI radiance with synergic use of AOD from MODIS and aerosol height from CALIOP. With the aerosol height and loading available from EPIC O_2 A and B bands, these closures are now possible with measurements from a single instrument.

The current algorithm incorporates a dust aerosol model and thus restricts its application to dust-laden scenes over a marine surface. The presence of nondust aerosols, such as transported biomass-burning smoke, could bias the retrieved AOD and ALH. The retrieval accuracy could also be affected by sea salt particles, though the impact tends to be small as sea salt particles usually place close to marine surface and have a much lower AOD than dust. Considering that the combined O_2 A and B bands can allow aerosol height retrieval over bright surface [*Sanghavi et al*., 2012] and that EPIC measurements in the UV and visible bands can be potentially used to discriminate aerosol types, a subsequent algorithm enhancement will include other aerosol types and land surfaces by utilizing more EPIC channels. Another limitation of the current algorithm exists for the case of multiple aerosol layers due to the assumption of a single Gaussian-like profile. This limitation is intrinsic to EPIC's narrow-band measurements that contain limited information for retrieving detailed aerosol vertical structure. Nevertheless, the retrieval of multiple-layered vertical distribution would be possible from hyperspectral radiometric and polarimetric measurements in the O_2 A and B bands [*Ding et al*., 2016], such as those measured by the Tropospheric Monitoring Instrument on board of the Copernicus Sentinel-5 Precursor satellite [*Sanders et al*., 2015].

Acknowledgments
This research is in part supported by NASA's DSCOVR Earth Science Algorithms Program (grant NNX17AB05G managed by Richard S. Eckman) and in part supported by Office of Naval Research (ONR's) Multidisciplinary University Research Initiatives (MURI) Program under the award N00014-16-1-2040, as well as NASA's GEO-CAPE science working group. We acknowledge the computational support from the High Performance Computing group at University of Iowa. All the data presented in this manuscript will be made available through Coalition on Publishing Data in the Earth and Space Sciences (https://copdessdirectory.osf.io) and please email J. Wang (jun-wang-1@uiowa.edu) and X. Xu (xiaoguang-xu@uiowa.edu) for details.

References

Babu, S. S., K. K. Moorthy, R. K. Manchanda, P. R. Sinha, S. K. Satheesh, D. P. Vajja, S. Srinivasan, and V. H. A. Kumar (2011), Free tropospheric black carbon aerosol measurements using high altitude balloon: Do BC layers build "their own homes" up in the atmosphere?, *Geophys. Res. Lett.*, *38*, L08803, doi:10.1029/2011GL046654.

Banks, J. R., H. E. Brindley, G. Stenchikov, and K. Schepanski (2017), Satellite retrievals of dust aerosol over the Red Sea and the Persian Gulf (2005–2015), *Atmos. Chem. Phys.*, *17*(6), 3987–4003.

Boesche, E., P. Stammes, and R. Bennartz (2009), Aerosol influence on polarization and intensity in near-infrared O_2 and CO_2 absorption bands observed from space, *J. Quant. Spectrosc. Radiat. Transfer*, *110*(3), 223–239.

Carlson, T. N., and J. M. Prospero (1972), The large-scale movement of Saharan air outbreaks over the northern equatorial Atlantic, *J. Appl. Meteorol.*, *11*(2), 283–297.

Cede A. and M. Kowalewski (2016), EPIC optical design, calibration, and data correction (talk), Abstract A21K-04 presented at 2016 Fall Meeting, AGU, San Francisco, Calif., 12-16 Dec.

Chance, K., and R. L. Kurucz (2010), An improved high-resolution solar reference spectrum for Earth's atmosphere measurements in the ultraviolet, visible, and near infrared, *J. Quant. Spectrosc. Radiat. Transfer*, *111*(9), 1289–1295.

Choi, J.-O., and C. E. Chung (2014), Sensitivity of aerosol direct radiative forcing to aerosol vertical profile, *Tellus B*, *66*, 24376.

Colarco, P. R., et al. (2003), Saharan dust transport to the Caribbean during PRIDE: 2. Transport, vertical profiles, and deposition in simulations of in situ and remote sensing observations, *J. Geophys. Res.*, *108*(D19), 8590, doi:10.1029/2002JD002659.

Ding, S., J. Wang, and X. Xu (2016), Polarimetric remote sensing in oxygen A and B bands: Sensitivity study and information content analysis for vertical profile of aerosols, *Atmos. Meas. Tech.*, *9*(5), 2077–2092.

Dubovik, O., et al. (2006), Application of spheroid models to account for aerosol particle nonsphericity in remote sensing of desert dust, *J. Geophys. Res.*, *111*, D11208, doi:10.1029/2005JD006619.

Dubuisson, P., R. Frouin, D. Dessailly, L. Duforêt, J.-F. Léon, K. Voss, and D. Antoine (2009), Estimating the altitude of aerosol plumes over the ocean from reflectance ratio measurements in the O2 A-band, *Remote Sens. Environ.*, *113*(9), 1899–1911.

Ge, C., J. Wang, and J. S. Reid (2014), Mesoscale modeling of smoke transport over the Southeast Asian Maritime Continent: Coupling of smoke direct radiative effect below and above the low-level clouds, *Atmos. Chem. Phys.*, *14*(1), 159–174, doi:10.5194/acp-14-159-2014.

Haney, C., D. Doelling, P. Minnis, R. Bhatt, B. Scarino, and A. Gopalan (2016), The calibration of the DSCOVR EPIC multiple visible channel instrument using MODIS and VIIRS as a reference, in *Proc. SPIE 9972, Earth Observing Systems XXI*, 99,720 pp., doi:10.1117/12.2238010.

Herman J., A. Szabo, and A. Marshak (2016), DSCOVR/EPIC: Calibration and related issues (talk), presented in DSCOVR EPIC & NISTAR Science Team Meeting, NASA Goddard Space Flight Center, Greenbelt, Md., 8-9 Feb.

Holben, B. N., et al. (1998), AERONET—A federated instrument network and data archive for aerosol characterization, *Remote Sens. Environ.*, *66*(1), 1–16.

Huang, J., C. Zhang, and J. M. Prospero (2010), African dust outbreaks: A satellite perspective of temporal and spatial variability over the tropical Atlantic Ocean, *J. Geophys. Res.*, *115*, D05202, doi:10.1029/2009JD012516.

Ichoku, C., D. A. Chu, S. Mattoo, Y. J. Kaufman, L. A. Remer, D. Tanré, I. Slutsker, and B. N. Holben (2002), A spatio-temporal approach for global validation and analysis of MODIS aerosol products, *Geophys. Res. Lett.*, *29*(12), 1616, doi:10.1029/2001GL013206.

Jeong, M.-J., and N. C. Hsu (2008), Retrievals of aerosol single-scattering albedo and effective aerosol layer height for biomass-burning smoke: Synergy derived from "A-Train" sensors, *Geophys. Res. Lett.*, *35*, L24801, doi:10.1029/2008GL036279.

Karyampudi, V. M., et al. (1999), Validation of the Saharan dust plume conceptual model using Lidar, Meteosat, and ECMWF data, *Bull. Am. Meteorol. Soc.*, *80*(6), 1045–1075.
Kipling, Z., et al. (2016), What controls the vertical distribution of aerosol? Relationships between process sensitivity in HadGEM3–UKCA and inter-model variation from AeroCom phase II, *Atmos. Chem. Phys.*, *16*(4), 2221–2241.
Koch, D. and A.D. Del Genio (2010), Black carbon semi-direct effects on cloud cover: Review and synthesis, *Atmos. Chem. Phys.*, *10*, 7685–7696.
Koelemeijer, R. B. A., J. de Haan, and P. Stammes (2003), A database of spectral surface reflectivity in the range 335–772 nm derived from 5.5 years of GOME observations, *J. Geophys. Res.*, *108*(D2), 4070, doi:10.1029/2002JD002429.
Koffi, B., et al. (2012), Application of the CALIOP layer product to evaluate the vertical distribution of aerosols estimated by global models: AeroCom phase I results, *J. Geophys. Res.*, *117*, D10201, doi:10.1029/2011JD016858.
Kokhanovsky, A. A., and V. V. Rozanov (2010), The determination of dust cloud altitudes from a satellite using hyperspectral measurements in the gaseous absorption band, *Int. J. Remote Sens.*, *31*(10), 2729–2744.
Koppers, G. A. A. and D. P. Murtagh (1997), Retrieval of height resolved aerosol optical thickness in the atmospheric band, in *Radiative Transfer in the Absorption Bands of Oxygen: Studies of Their Significance in Ozone Chemistry and Potential for Aerosol Remote Sensing*, edited by G. A. A. Koppers, pp. 1–24, Stockholm Univ., Stockholm, Sweden.
Levy, R. C., L. A. Remer, D. Tanré, Y. J. Kaufman, C. Ichoku, B. N. Holben, J. M. Livingston, P. B. Russell, and H. Maring (2003), Evaluation of the Moderate-Resolution Imaging Spectroradiometer (MODIS) retrievals of dust aerosol over the ocean during PRIDE, *J. Geophys. Res.*, *108*(D19), 8594, doi:10.1029/2002JD002460.
Levy, R. C., S. Mattoo, L. A. Munchak, L. A. Remer, A. M. Sayer, F. Patadia, and N. C. Hsu (2013), The collection 6 MODIS aerosol products over land and ocean, *Atmos. Meas. Tech.*, *6*, 2989–3034.
Maring, H., D. L. Savioe, M. A. Izaguirre, L. Custals, and J. S. Reid (2003), Vertical distributions of dust and sea-salt aerosols over Puerto Rico during PRIDE measured from a light aircraft, *J. Geophys. Res.*, *108*(D19), 8587, doi:10.1029/2002JD002544.
Marshak, A., and Y. Knyazikhin (2017), The spectral invariant approximation within canopy radiative transfer to support the use of the EPIC/DSCOVR oxygen B-band for monitoring vegetation, *J. Quant. Spectrosc. Radiat. Transfer*, *191*, 7–12.
Martins, J. V., D. Tanré, L. Remer, Y. Kaufman, S. Mattoo, and R. Levy (2002), MODIS cloud screening for remote sensing of aerosols over oceans using spatial variability, *Geophys. Res. Lett.*, *29*(12), 1619, doi:10.1029/2001GL013252.
Pflug, B. M., and T. Ruppert (1993), Information content of measurements in the O2A- and O2B-bands for monitoring of aerosols from space, *SPIE Atmos. Propag. Remote Sens. II*, *1968* 533–544.
Prospero, J. M., and T. N. Carlson (1972), Vertical and areal distribution of Saharan dust over the western equatorial north Atlantic Ocean, *J. Geophys. Res.*, *77*(27), 5255–5265, doi:10.1029/JC077i027p05255.
Prospero, J. M., P. Ginoux, O. Torres, S. E. Nicholson, and T. E. Gill (2002), Environmental characterization of global sources of atmospheric soil dust identified with the NIMBUS 7 Total Ozone Mapping Spectrometer (TOMS) absorbing aerosol product, *Rev. Geophys.*, *40*(1), 1002, doi:10.1029/2000RG000095.
Reid, J. S., et al. (2003), Analysis of measurements of Saharan dust by airborne and ground-based remote sensing methods during the Puerto Rico Dust Experiment (PRIDE), *J. Geophys. Res.*, *108*(D19), 8586, doi:10.1029/2002JD002493.
Reid, J.S., D. L. Westphal, J. Livingston, D. S. Savoie, H. B. Maring, P. Pilewskie, D. Eleuterio (2002), The vertical distribution of dust transported into the Caribbean during the Puerto Rico Dust Experiment, *Geophys. Res. Lett.*, *29*(7), 1151, doi:10.1029/2001GL014092.
Remer, L. A., et al. (2005), The MODIS aerosol algorithm, products, and validation, *J. Atmos. Sci.*, *62*(4), 947–973.
Rothman, L. S., et al. (2009), The HITRAN 2008 molecular spectroscopic database, *J. Quant. Spectrosc. Radiat. Transfer*, *110*(9–10), 533–572.
Samset, B. H., et al. (2013), Black carbon vertical profiles strongly affect its radiative forcing uncertainty, *Atmos. Chem. Phys.*, *13*(5), 2423–2434.
Sanders, A. F. J., J. F. de Haan, M. Sneep, A. Apituley, P. Stammes, M. O. Vieitez, L. G. Tilstra, O. N. E. Tuinder, C. E. Koning, and J. P. Veefkind (2015), Evaluation of the operational aerosol layer height retrieval algorithm for Sentinel-5 precursor: Application to O2 A band observations from GOME-2A, *Atmos. Meas. Tech.*, *8*(11), 4947–4977.
Sanghavi, S., J. V. Martonchik, J. Landgraf, and U. Platt (2012), Retrieval of aerosol optical depth and vertical distribution using O2 A- and B-band SCIAMACHY observations over Kanpur: A case study, *Atmos. Meas. Tech.*, *5*(5), 1099–1119.
Satheesh, S. K., K. K. Moorthy, S. S. Babu, V. Vinoj, and C. B. S. Dutt (2008), Climate implications of large warming by elevated aerosol over India, *Geophys. Res. Lett.*, *35*, L19809, doi:10.1029/2008GL034944.
Sears, T. M., G. E. Thomas, E. Carboni, A. J. A. Smith and R. G. Grainger (2013), SO_2 as a possible proxy for volcanic ash in aviation hazard avoidance, *J. Geophys. Res. Atmos.*, *118*, 5698–5709, doi:10.1002/jgrd.50505.
Spurr, R. (2006), VLIDORT: A linearized pseudo-spherical vector discrete ordinate radiative transfer code for forward model and retrieval studies in multilayer multiple scattering media, *J. Quant. Spectrosc. Radiat. Transfer*, *102*, 316–342.
Spurr, R., and M. Christi (2014), On the generation of atmospheric property Jacobians from the (V)LIDORT linearized radiative transfer models, *J. Quant. Spectrosc. Radiat. Transfer*, *142*, 109–115.
Torres O., R. C. Levy, L. Remer, H. Jethva, and J. Wang (2016), Aerosol particle properties using EPIC UV-VIS observations (talk), presented in *DSCOVR Earth Science Team Meeting*, NASA Goddard Space Flight Center, Greenbelt, Md., Oct 31 – Nov 1.
Torres, O., P. K. Bhartia, J. R. Herman, Z. Ahmad, and J. Gleason (1998), Derivation of aerosol properties from satellite measurements of backscattered ultraviolet radiation: Theoretical basis, *J. Geophys. Res.*, *103*(D14), 17,099–17,110, doi:10.1029/98JD00900.
Wang, J., S.A. Christopher, J.S. Reid, H. Maring, D. Savoie, B.H. Holben, J.M. Livingston, P.B. Russell, and S.K. Yang (2003), GOES-8 retrieval of dust aerosol optical thickness over the Atlantic Ocean during PRIDE, *J. Geophys. Res.*, *108*(D19), 8595, doi:10.1029/2002JD002494.
Wang, J., X. Xu, S. Ding, J. Zeng, R. Spurr, X. Liu, K. Chance, and M. Mishchenko (2014), A numerical testbed for remote sensing of aerosols, and its demonstration for evaluating retrieval synergy from a geostationary satellite constellation of GEO-CAPE and GOES-R, *J. Quant. Spectrosc. Radiat. Transfer*, *146*, 510–528.
Wendisch, M., et al. (2008), Radiative and dynamic effects of absorbing aerosol particles over the Pearl River Delta, China, *Atmos. Environ.*, *42*(25), 6405–6416.
Winker, D. M., M. A. Vaughan, A. Omar, Y. Hu, K. A. Powell, Z. Liu, W. H. Hunt, and S. A. Young (2009), Overview of the CALIPSO mission and CALIOP data processing algorithms, *J. Atmos. Oceanic Technol.*, *26*(11), 2310–2323.
Xu X., J. Wang, J. Zeng, R. Spurr, X. Liu, O. Dubovik, L. Li, Z. Li, M. I. Mishchenko, A. Siniuk, and B. N. Holben (2015), Retrieval of aerosol microphysical properties from AERONET photopolarimetric measurements: 2. A new research algorithm and case demonstration, *J. Geophys. Res. Atmos.*, *120*, 7079–7098, doi:10.1002/2015JD023113.
Xu X., J. Wang, Y. Wang, and A. Kokhanovsky (2017), Passive remote sensing of aerosol height, in *Remote Sensing of Aerosols, Clouds, and Precipitation*, edited by T. Islam et al., Elsevier, Amsterdam, doi:10.1016/B978-0-12-810437-8.00001-3.

Yang, Y., A. Marshak, J. Mao, A. Lyapustin, and J. Herman (2013), A method of retrieving cloud top height and cloud geometrical thickness with oxygen A and B bands for the Deep Space Climate Observatory (DSCOVR) mission: Radiative transfer simulations, *J. Quant. Spectrosc. Radiat. Transfer*, *122*, 141–149.

Young, S. A., and M. A. Vaughan (2009), The retrieval of profiles of particulate extinction from Cloud-Aerosol Lidar Infrared Pathfinder Satellite Observations (CALIPSO) data: Algorithm description, *J. Atmos. Oceanic Technol.*, *26*(6), 1105–1119.

Yu, H., M. Chin, D. M. Winker, A. H. Omar, Z. Liu, C. Kittaka, and T. Diehl (2010), Global view of aerosol vertical distributions from CALIPSO lidar measurements and GOCART simulations: Regional and seasonal variations, *J. Geophys. Res.*, *115*, D00H30, doi:10.1029/2009JD013364.

Yu, H., et al. (2015), Quantification of trans-Atlantic dust transport from seven-year (2007–2013) record of CALIPSO lidar measurements, *Remote Sens. Environ.*, *159*, 232–249.

Zeng, J., Q. Han, and J. Wang (2008), High-spectral resolution simulation of polarization of skylight: Sensitivity to aerosol vertical profile, *Geophys. Res. Lett.*, *35*, L20801, doi:10.1029/2008GL035645.

Zhang, L., Q. B. Li, Y. Gu, K. N. Liou, and B. Meland (2013), Dust vertical profile impact on global radiative forcing estimation using a coupled chemical-transport–radiative-transfer model, *Atmos. Chem. Phys.*, *13*(14), 7097–7114, doi:10.5194/acp-13-7097-2013.

Zhu, A., V. Ramanathan, F. Li, and D. Kim (2007), Dust plumes over the Pacific, Indian, and Atlantic Oceans: Climatology and radiative impact, *J. Geophys. Res.*, *112*, D16208, doi:10.1029/2007JD008427.

Erratum

In the originally published version of this article, the text in Figure 4 was mislabeled CALIPSO: 2014-04-17 14:18 UTC (panel a) and CALIPSO: 2014-04-18 15:02 UTC (panel b). The year for both has been changed from 2014 to the correct year 2016, and this version may be considered the authoritative version of record.